Advanced Composite Materials
Publication details, including instructions for authors and subscription information:
http://www.tandfonline.com/loi/tacm20

Damage analysis of CFRP plates exposed to cryogenic shock by AE monitoring

Yoshihiro Mizutani , Taketo Hiratsuka , Hidenori Tanabe & Mikio Takemoto

Version of record first published: 02 Apr 2012.

To cite this article: Yoshihiro Mizutani , Taketo Hiratsuka , Hidenori Tanabe & Mikio Takemoto (2005): Damage analysis of CFRP plates exposed to cryogenic shock by AE monitoring, Advanced Composite Materials, 14:1, 99-111

To link to this article: http://dx.doi.org/10.1163/1568551053297094

Adv. Composite Mater., Vol. 14, No. 1, pp. 99–111 (2005)

Also available online - www.vsppub.com

Damage analysis of CFRP plates exposed to cryogenic shock by AE monitoring

YOSHIHIRO MIZUTANI [1,*], TAKETO HIRATSUKA [2], HIDENORI TANABE [2] and MIKIO TAKEMOTO [2]

[1] *Department of Mechanical Science and Engineering, Graduate School of Science and Engineering, Tokyo Institute of Technology, 2-12-1-I1-70, O-okayama, Meguroku, Tokyo 152-8552, Japan*
[2] *Department of Mechanical Engineering, Graduate School of Science and Engineering, Aoyama Gakuin University, 5-10-1, Fuchinobe, Sagamihara, Kanagawa 229-8558, Japan*

Received 20 July 2004; accepted 1 October 2004

Abstract—The progression of micro-fractures in carbon fiber reinforced composite (CFRP) plates subjected to cryogenic thermal shock was studied by acoustic emission (AE). Thermal shocks were given by putting liquefied nitrogen into a cell mounted on the upper surface of the specimens with different matrix resins. No damage was observed in the specimen with heat-resistant resin, while three hundred AE counts were detected in the specimen with conventional resin, in which many matrix cracks were observed from the small temperature differences in the wall. AE signals were classified into three fractures types, namely, delaminations and matrix and transverse cracks, by waveform characterization. Here, the three AE signal types were simulated by adiabatic thermal expansion with a pulse laser. The numbers of all three types of AE signals linearly increased with time. AEs from the matrix cracks were more frequent than those from delaminations and transverse cracks.

Vertical immersion testing of the CFRP plate into liquefied nitrogen revealed only matrix cracks on the specimen surface at temperatures higher than 228 K. At 213 K, a large number of AE signals due to matrix cracks but few signals due to delaminations and transverse cracks were observed. At 77 K, a large number of AE signals due to the three types of fractures were observed.

Keywords: CFRP; acoustic emission; cryogenic thermal shock; fracture modes; signal classification; pulse YAG-laser.

1. INTRODUCTION

Reducing the weight of cryogenic fuel tanks is a key objective for future aerospace transportation systems. The applicability of lightweight carbon fiber reinforced composite (CFRP) materials to such tanks has been studied [1–4], and a database

*To whom correspondence should be addressed. E-mail: ymizutan@mes.titech.ac.jp

of the mechanical properties of CFRPs at cryogenic temperatures is being assembled [5], though some studies on the cryogenic thermal shock resistance are reported. Progression of micro-fractures in CFRPs by cryogenic thermal shock needs to be studied using advanced non-destructive monitoring techniques.

Acoustic emission (AE) is a powerful tool for monitoring fracture progression and fracture types. Four types of fracture, such as fiber breakages, delaminations, and matrix and transverse cracks, are reported to occur and produce AE signals with different waveforms [6]. Kinjo *et al.* [7] studied fracture progression in tensile-loaded GFRP coupons by classifying AE signals. Computer simulation of AE signals from different types of fracture or different source locations in a distal plane have been reported [8–10]. We simulated four types of fractures by the adiabatic thermal expansion of a pulse YAG laser. The characteristics of AE signals from different fracture types were successfully classified by this method; and we have studied the progression of fracture types in CFRP plates during in-plane compression testing [11].

In this study, the progression of fracture types in CFRP plates subjected to cryogenic shock is studied utilizing AE. The effects of both cooling temperature and temperature distribution in CFRP plates on the fracture types and progression are studied.

2. SPECIMENS AND EXPERIMENTAL METHOD

Table 1 shows the material specifications of the two types of CFRP plates, TypesA and B, used in this study. PAN-based carbon fibers are used in Type-A specimen, while PITCH-based fibers are used in Type-B. The matrix of both specimens are thermosetting epoxy, with thermal resistance epoxy (Toho Tenax Co., Ltd., Type #133) was used for Type-A, and conventional epoxy for Type-B. The stacking sequences of both specimens are different since they are not produced in a laboratory.

Figure 1 shows the experimental setup. Local thermal shock is given to the specimen by putting 250 ml of liquefied nitrogen (LN_2) into an aluminum cell (diameter 50 mm) mounted on the upper surface of the plate center. Temperatures at both sides of points A, B and C are monitored by thermo-couples. Internal damage due to the thermal shock was monitored by two AE sensors (PAC, type: PICO with

Table 1.
Description of two types of specimens

	Type-A	Type-B
Prepreg sheet	IM600/#133 (TOHO TENAX)	XN-50 (Nippon Graphite Fiber)
Carbon fiber	PAN based	Pitch based
Layer construction	$[\pm 45°/90°_2/\pm 45°/90°_2/\pm 45°]$	$[0°_6/90°_6]_{sym.}$
Thickness (mm)	1.2	2.4

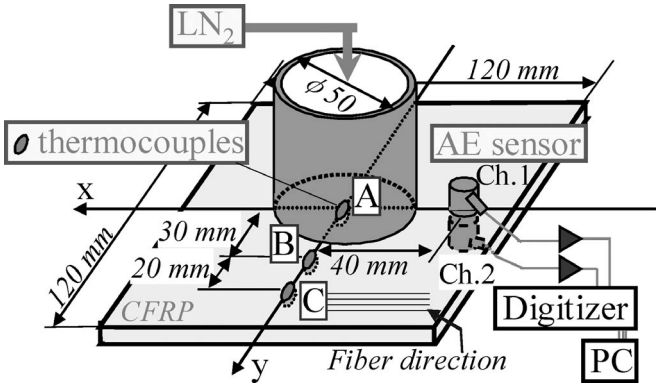

Figure 1. Schematic illustration of cryogenic shock testing. The cell wasmounted on the upper surface and filled with liquefied nitrogen.

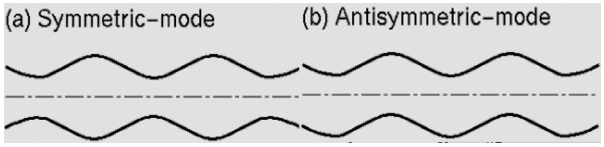

Figure 2. Schematic illustration of Lamb (plate) wave propagation.

a center frequency of 450 kHz) mounted 40 mm from the center on both surfaces. AE can be detected as the dispersive Lamb (plate) wave; it has two modes, anti-symmetric (A-) and symmetric (S-) (Fig. 2). The wave mode of detected AE signals is important for fracture type classification and for determinations comparing the polarity of sensor outputs. Here, the same polarity designates S-mode, while the opposite designates A-mode.

AE monitoring was started before the LN_2 was introduced into the cell and was stopped after the evaporation of all LN_2, at which point no AE was detected. After this testing, a fluorescent penetrant test was conducted to inspect the surface matrix cracks.

3. RESULTS OF THE THERMAL SHOCK TEST

Figures 3 and 4 show the results of fluorescent penetrant testing of Type-A and Type-B specimens. No damage was observed in Type-A specimen (Fig. 3). Note that the ring- shaped indication on the back surface is the remains of adhesives used in other experiments. As opposed to the Type-A specimen, the Type-B specimen suffered 39 matrix cracks on both surfaces, as shown in Figs 4 and 5.

Another experiment for a Type-A specimen again produced no damage, but two other experiments for Type-B specimen produced 18 and 20 matrix cracks, respectively.

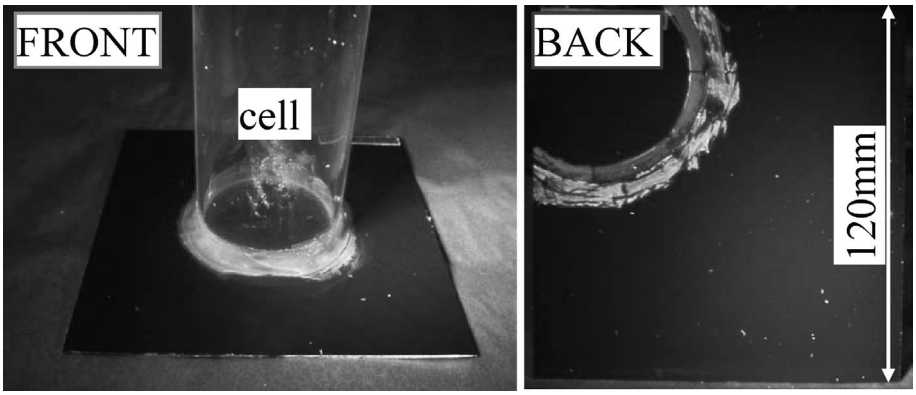

Figure 3. Results of the penetrant fluorescent test of Type-A specimen.

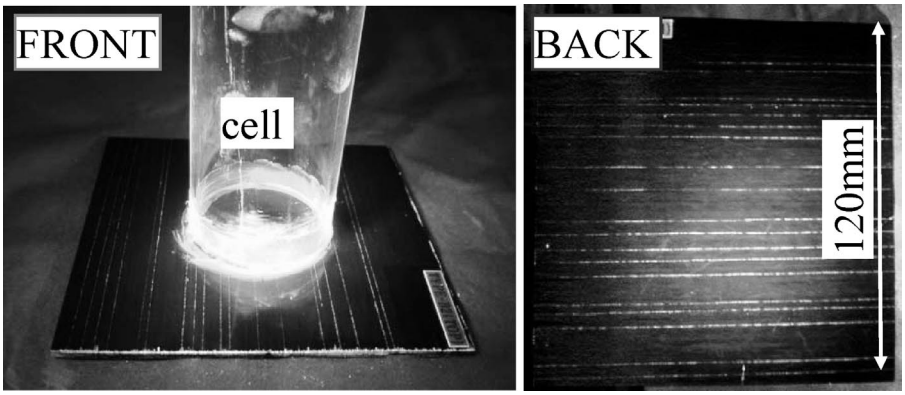

Figure 4. Surface matrix cracks on a Type-B CFRP plate revealed by penetrant fluorescent test.

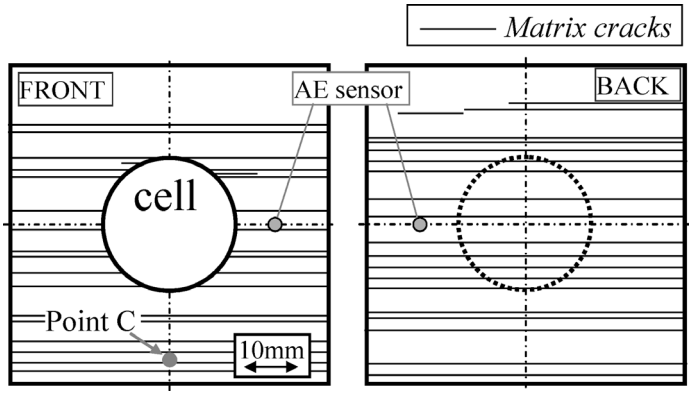

Figure 5. Schematic illustration of matrix cracks observed for a Type-B specimen.

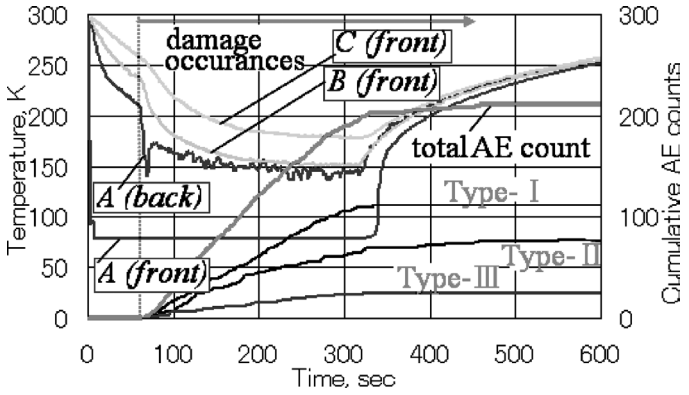

Figure 6. Temperature histories at points A, B and C with cumulative AE counts.

We monitored 30 AE events for the Type-A test, and 380 events for the first Type-B specimen test. Most AE events from the Type-A specimen were detected shortly after pouring the LN_2 and were found to be secondary AEs from the boiling of LN_2 or from the sensor due to temperature changes. Conversely, a large number of AE events were continuously detected from the Type-B specimen; for these we studied the relationship between temperature history and AE occurrence. Figure 6 shows the cumulative AE events as a function of temperature at locations A, B and C in Fig. 1. LN_2 was poured into the cell from the 60 second to the 110 second time points. AE signals were continuously detected until 746 seconds, even after the nitrogen had fully evaporated at the 694 seconds time point.

After the test, 39 matrix cracks were observed at points all over the specimen surfaces, including point C where the temperature decreased to only 200 K at minimum. It is noted that the location C suffered matrix cracking in spite of the small temperature drop there to just 200 K and there being just a small temperature difference in the wall. Another key feature is that the matrix cracks occurred on both surfaces; taken together, these facts indicate that the matrix cracking occurred not by the temperature differences across the specimen wall, but by the embrittlement of the matrix or by the in-plane temperature difference.

We next studied fracture timing and types. We first separated noises from detected AE events and then classified the events into three waveform types (Types I to III), as shown in Fig. 7. AE signals detected by the Ch.1 sensor on the upper surface are shown on the left side, and signals detected by the Ch.2 sensor are on the right. Detected times are shown at the upper right of the signals.

A Type-I signal contains a weak S_0-component, followed by a strong A_0-mode. A Type-II signal is characterized by a S_0-component with an amplitude larger than that of the A_0-mode that follows. A Type-III signal appears to be of a single mode (namely the S_0-mode) containing approximately the same frequency components.

We next prepared AE signals utilizing three artificial fractures (delamination, and matrix and transverse cracks) produced by a pulse-laser (pulse duration of 5 ns)

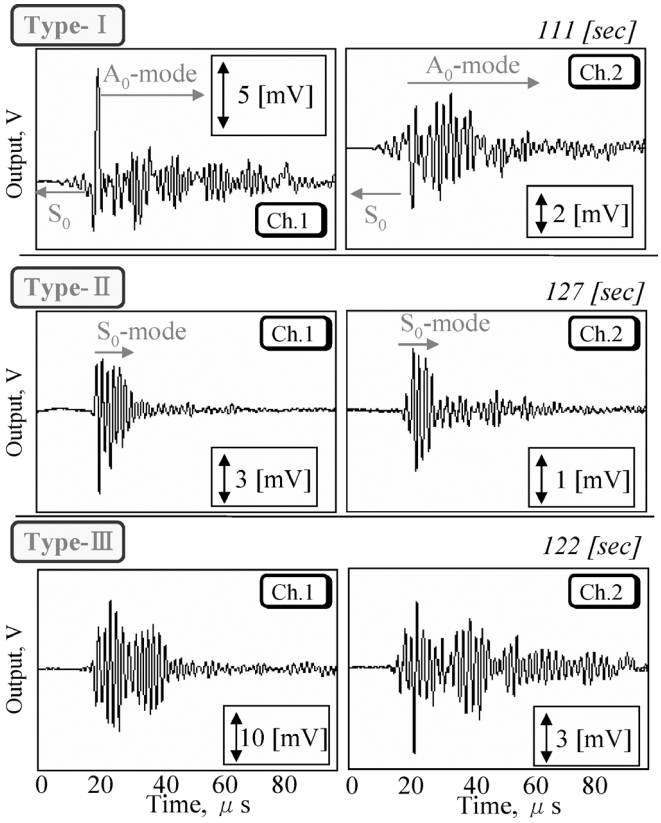

Figure 7. Three types of AE signals detected for Type-B specimen.

irradiation on the surface and a cross-section of the specimen. Details of the simulation method can be found elsewhere [11].

AE due to the matrix crack (abbreviated as MC) is produced by focusing a line-shaped pulse laser on the specimen surface as the laser line coincides with the surface fiber direction. Adiabatic thermal expansion in the normal direction of the laser line simulates the matrix crack. Delamination along the interface of the inner layers was simulated by focusing a line laser on the distal plane of the specimen. Simulation of a transverse crack is much more difficult and is accomplished by superposing the AE signals produced by a point-focused laser irradiation at the second 90 degree layer by a 0.1 mm step.

Figure 9 shows the simulated AE signal. It is predicted that the matrix crack produces an A_0-Lamb wave with a large amplitude, while the delamination produces a large amplitude S_0-mode. AE due to the transverse crack is characterized by a single mode (namely the S_0-mode) containing approximately the same frequency. These three AE signals correspond to the AE signals from Type-I, Type-II and Type-III fractures in Fig. 7.

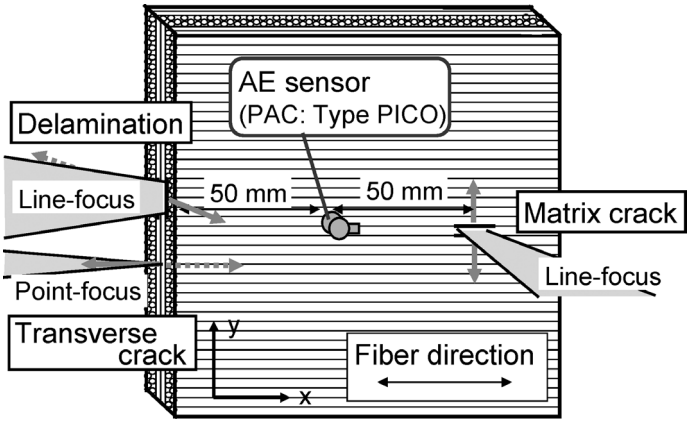

Figure 8. AE monitoring of an artificial fracture produced by pulse laser.

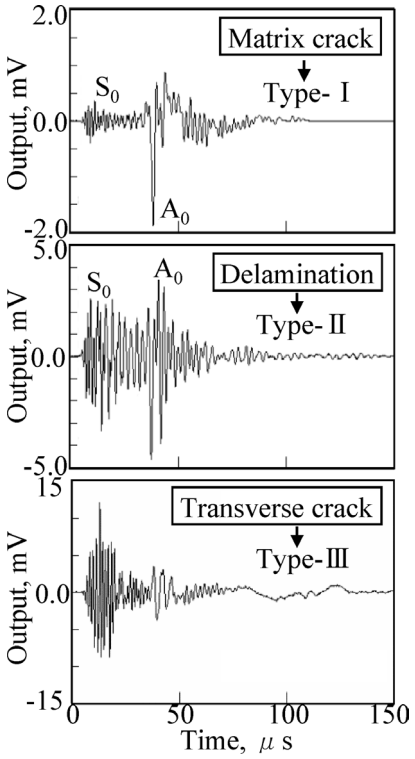

Figure 9. AE signals from three types of artificial fractures.

On the basis of the characteristics of these signals, we classified the AE events detected into one of three fracture types. Figure 10 represents the cumulative AE counts of the three fracture modes. A large number of Type-I signals from matrix cracks were realized. Type-II (Delamination) and Type-III (Transverse Crack)

AE signals were five and six times smaller than those from the matrix cracks. Detailed analyses showed that Type-II and Type-III signals were produced after the generation of Type-I signals. Figure 12 shows the postmortem cross-section of

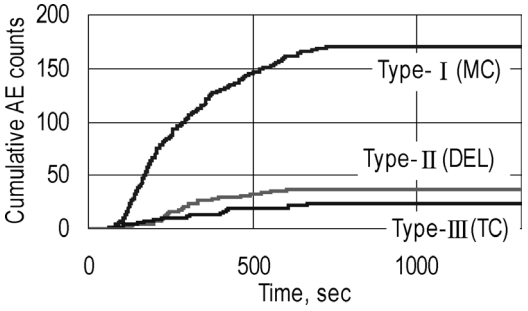

Figure 10. Cumulative AE counts of three fracture types. MC: Matrix crack, DEL: Delamination, TC: Transverse crack.

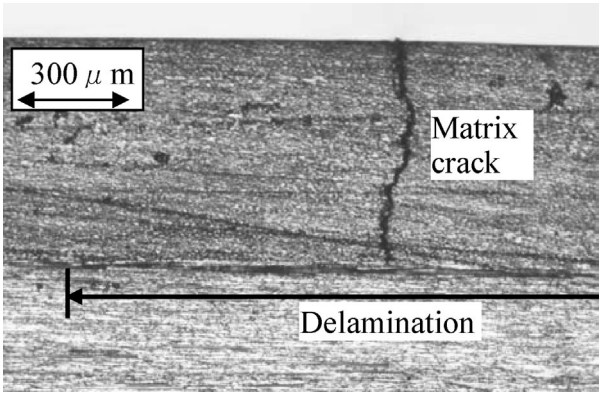

Figure 11. Cross-section of damaged Type-B CFRP plate.

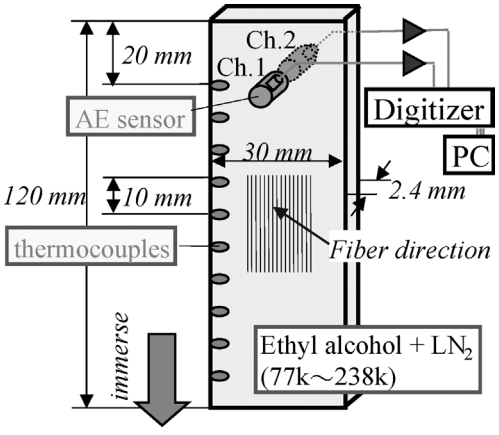

Figure 12. Experimental setup for vertical immersion test.

a Type-B specimen. Both a matrix crack and interlaminar delamination can be seen while a transverse crack cannot be detected. We concluded that an internal fracture occurs in the sequence of (1) matrix cracks on both surfaces, (2) delamination and (3) transverse cracks.

4. RESULTS FROM VERTICAL IMMERSION TESTS OF CFRP COUPONS

The test described in the previous section suggested that the damage was not produced by the temperature differences across the specimen wall, but by matrix embrittlement or by the in-plane temperature distribution. To demonstrate this, we investigated damage progression in a specimen immersed vertically into the low temperature liquid. As shown in Fig. 12, Type-B specimens (length 120 mm, width 30 mm, thickness 2.4 mm) were immersed in the mixed solution of ethanol and liquid nitrogen with boiling temperatures from 77 K to 238 K. Immersion tests were conducted by changing the immersion velocity and immersion depth, as shown in Table 2. AE sensors are mounted on both surfaces at 20 mm from the upper edge, and thermocouples are put on one surface at 10 mm intervals.

Figure 13 shows the surface cracks of the specimen immersed into 213 K and 77 K solutions at velocities of 25 mm/s to 50 mm depth. At 213 K, only one matrix crack of 80 mm length was observed, while five matrix cracks were observed on both surfaces at 77 K. Results from another test are shown in Table 2. No crack

Table 2.
Relationships between immersed conditions and damage

Cooling temperature	Imersion speed	Imersion depth	Length and number of matrix craks
238 K	25 mm/s	50 mm	no damage
233 K	25 mm/s	50 mm	no damage
228 K	25 mm/s	50 mm	28 mm × 1
			3 mm × 1
223 K	25 mm/s	50 mm	45 mm × 1
218 K	25 mm/s	50 mm	69 mm × 1
			22 mm × 1
213 K	25 mm/s	20 mm	no damage
	25 mm/s	50 mm	80 mm × 1
	25 mm/s	80 mm	120 mm × 1
			90 mm × 1
			65 mm × 1
	1.7 mm/s	50 mm	96 mm × 1
77 K	25 mm/s	50 mm	120 mm × 2
			90 mm × 1
			14 mm × 1
			12 mm × 1

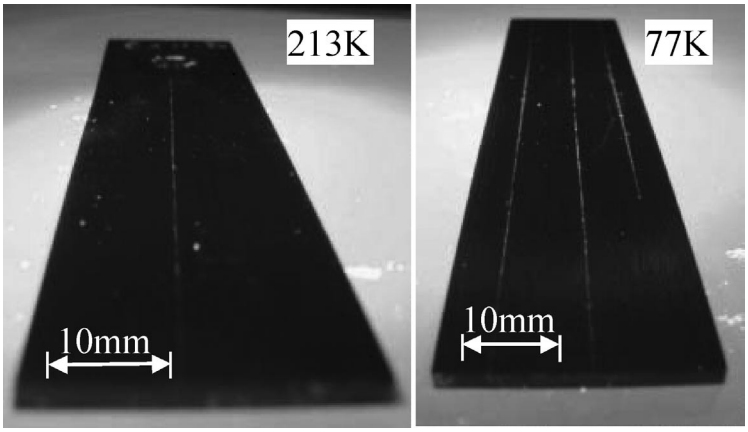

Figure 13. Surface cracks on the type-B specimen after vertical immersion test. Immersion velocity: 25 mm/s, immersion depth: 50 mm.

was observed at a temperature higher than 233 K. The numbers and lengths of the matrix cracks were drastically changed in solution temperatures lower than 233 K. These results strongly suggest that the low-temperature embrittlement of the matrix resin is the cause of the matrix cracks. In-plane temperature difference is supposed to be the driving force producing the fractures, since material embrittlement does not lead to cracking.

The temperature histories in the longitudinal direction during vertical immersion are shown in Figs 14 and 15. Here, $y = 20$ designates the location 20 mm from the bottom of the specimen. The maximum temperature differences (as Dif) and cumulative AE counts are also shown in the figures. For the 213 K test (Fig. 14), a large number of AEs were detected during the first 100 s, during which the maximum temperature differences were consistently higher than 50 K. After the 100-s time point, the maximum temperature differences became smaller, and as a result few AEs were detected. For the 77 K test (Fig. 15), the in-plane temperature difference was higher than 110 K throughout the time, and cumulative AE counts linearly increased with time due to the maximum acquisition rate of the AE system used.

Fracture types were classified by modal analysis of the AE signals. Type-I fractures (matrix cracks) are found to be major in the 228 K and 213 K tests, while in the 77 K test three types of AE signals were observed. Figure 16 shows a cross-section of the specimen subjected to the 77 K test. Both transverse cracks and delaminations are observed. Cumulative AE counts of Types I to III during the 213 K and 77 K tests are shown in Figs 17 and 18, respectively. In the 213 K test, Type-I fractures are dominant, while Type-II and Type-III fractures are observed in the 77 K test. These results agree well with the postmortem observation in Fig. 16. It was concluded that surface matrix cracks occur when the surface temperature reaches a critical temperature. Following a matrix crack, both delaminations and

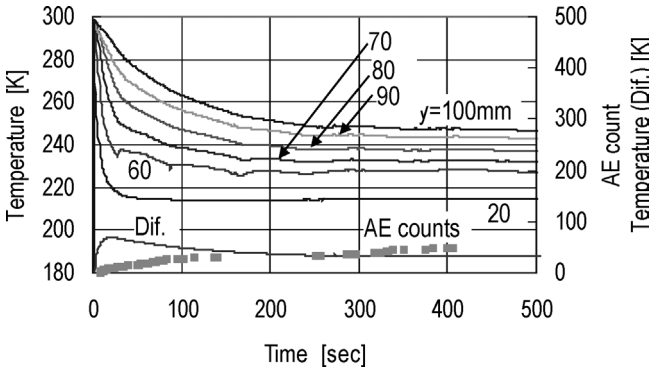

Figure 14. Changes of temperature and temperature differences with AE counts during the cooling of a CFRP plate to 213 K.

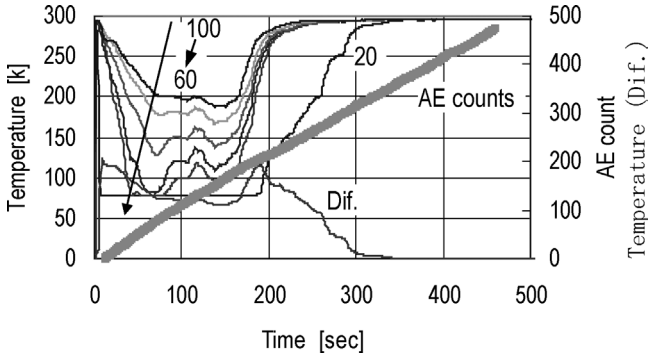

Figure 15. Changes of temperature and differences of temperature with AE counts during cooling an CFRP plate to 77 K.

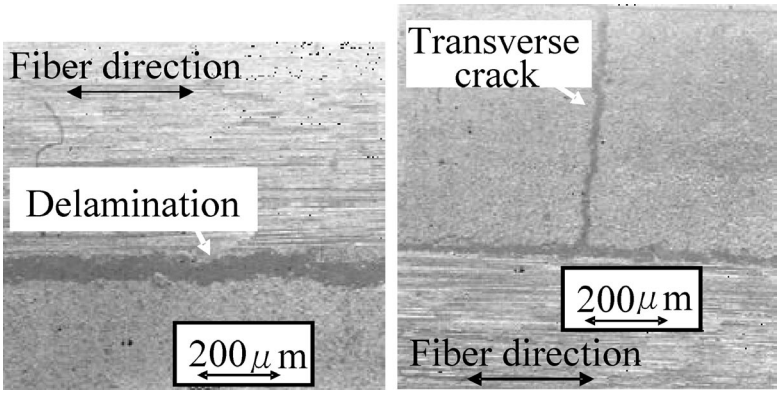

Figure 16. Cross-section of CFRP immersed in liquid nitrogen at 77 K.

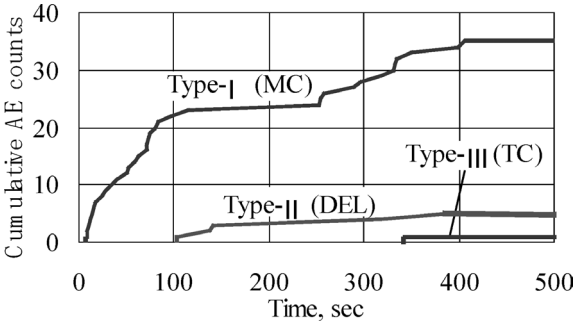

Figure 17. Cumulative AE counts of three fracture types. Temp.: 213 K, immersion velocity: 25 m/s, immersion depth: 50 mm.

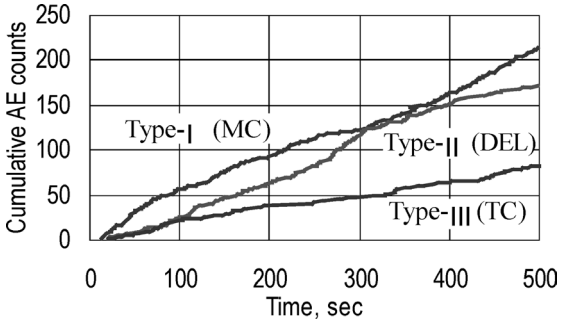

Figure 18. Cumulative AE counts of three fracture types. Temp.: 77 K, immersion velocity: 25 mm/s, immersion depth: 50 mm.

transverse cracks occur when the temperature becomes much lower and the in-plane temperature difference becomes larger.

5. CONCLUSION

Cryogenic thermal shock testing was conducted for two types of CFRP plates (Types A and B) with different matrix resins. The progression of micro-fractures was monitored by acoustic emission (AE). The influences on the damage from both cooling temperature and in-plane temperature differences are also studied.

The results can be summarized as:

(1) No damage was observed in a Type-A specimen made from heat-resistant resin.

(2) Three types of crack, namely, delamination, and matrix and transverse cracks, were observed for the Type-B test made from conventional resin. Damage was induced first by the matrix embrittlement and then by in-plane temperature differences.

(3) Vertical immersion of specimens into a low temperatures solution produced no cracks at temperatures higher than 233 K. From 228 K to 213 K, only

matrix cracks were produced, while at 77 K, three types of fractures were produced. In-plane temperature differences serve to generate fractures in embrittled matrix.

Acknowledgements

Professor Ono of UCLA provided valuable advice regarding the waveform classification and fracture simulations. Dr. Cho of Aoyama Gakuin University supported the thermal shock experiments. Dr. Morino of JAXA provided valuable information about cryogenic thermal shock testing.

REFERENCES

1. Final Report of the X-33 Liquid Hydrogen Tank Test Investigation Team. National Aeronautics and Space Administration, George C. Marshall Space Flight Center, Huntsville, Alabama 35812 (2000).
2. http://www.jaxa.jp/missions/projects/rockets/lng/index_j.html
3. S. Morino, T. Shimoda, T. Morimoto, T. Ishikawa and T. Aoki, Applicability of CFRP materials to the cryogenic propellant tank for reusable launch vehicle (RLV), *Adv. Composite Mater.* **10** (4), 339–347 (2001).
4. T. Shimoda, J. He and Y. Morino, Study of CFRP Application to Cryogenic Fuel Tank for RLV, in: *23rd Int. Sympos. on Space Technology and Science*, ISTS2002-c-13 (2002).
5. http://www.nal-acdb.com/
6. H. Suzuki, M. Takemoto and K. Ono, The fracture dynamics in a dissipative glass-fiber/epoxy model composite with AE source wave analysis, *J. AE* **14** (1), 35–50 (1996).
7. T. Kinjo, H. Suzuki, M. Takemoto and K. Ono, Fracture model classification using wavelet transformed AE signals from a composite, *J. AE* **15** (1), 19–32 (1997).
8. W. H. Prosser, Finite element and plate theory modeling of acoustic emission waveforms, *J. NDE* **18** (3), 83–90 (1999).
9. E. R. Green, Acoustic emission in composite laminates, *J. NDE* **17** (3), 117–127 (1998).
10. W. H. Prosser, M. A. Hamstad, J. Gray and A. O'Gallagher, Reflections of AE waves in finite plates: finite element modeling and experimental measurements, *J. AE* **17** (1-2), 37–47 (1999).
11. Y. Mizutani, K. Nagashima, M. Takemoto and K. Ono, Fracture mechanism characterization of cross-ply carbon-fiber composites using acoustic emission analysis, *NDTE Int.* **33**, 101–110 (2000).